RSC Advances

PAPER

Published on 18 August 2026

Cite this: DOI: 10.1039/d6ra05617b

Ultrasound-assisted synthesis of benzazole-based imidate derivatives: a DFT investigation of the thermodynamic stability and electronic properties of the synthesized products

Yavar Ahmadi, *[a] Manijeh Nematpour [a] and Mohammad Qasemnazhand*[b]

A rapid, efficient, and simple ultrasonic-assisted protocol is reported herein for the synthesis of benzazoles bearing an imidate skeleton *via* the one-pot reaction of isocyanides, various alcohols, and benzo(thiazole-oxazole-imidazole) using Cs_2CO_3 as an active base, a THF solvent, and a copper catalyst, without the use of additional ligands under ultrasonic conditions for 50 minutes with good efficiency. The role of ultrasound in this reaction is to reduce the reaction time, increase the efficiency of product preparation, and simplify the work-up process. The use of simple and available raw materials, mild copper catalytic reaction conditions, easy purification with the help of solvents, and finally the synthesis of 12 new compounds from benzazoles with an imidate skeleton are the notable features of this protocol. Moreover, in this study, density functional theory (DFT) calculations were performed to investigate the thermodynamic stability and electronic properties of benzazole derivatives containing different heteroatoms (X = O, S, N–H, and N–CH_3) in THF using the SMD solvation model. The calculated thermodynamic parameters reveal that all the investigated systems are enthalpically stabilized, while the negative entropy contributions partially offset this stabilization. Among the studied derivatives, the N–H system exhibits the most favorable Gibbs free energy, whereas the oxygen-containing derivative shows a larger entropic penalty. Frontier molecular orbital analysis indicates that heteroatom substitution significantly affects the electronic structure of the benzazole framework. The HOMO–LUMO energy gap decreases upon replacing the *N*-methyl group with the oxygen substituent, accompanied by an increase in electrophilicity and more negative chemical potential values. These results demonstrate that the nature of the heteroatom plays an important role in controlling the thermodynamic stability and electronic reactivity of benzazole derivatives in solution.

Received 25th June 2026
Accepted 5th August 2026

DOI: 10.1039/d6ra05617b

rsc.li/rsc-advances

Introduction

Benzazoles are heterocycles containing nitrogen, sulfur, and oxygen atoms, and they are often found in a variety of natural products and pharmaceutical agents.[1–3] These heterocycles can be used as new building blocks for the synthesis of more useful heterocycles because of their special chemical structure.[4] Heterocyclic compounds containing a benzazole structure exhibit a wide range of pharmacological activities such as anticancer, anti-tubercular, anti-microbial, anti-tumor, analgesic, anti-leishmanial, and anti-inflammatory properties.[5–9]

Due to the vast scope and application of biological activities investigated, benzazole derivatives have received the greatest importance in medicinal chemistry research and organic compound synthesis.[10] Therefore, it is highly desirable to develop necessary, appropriate, and low-risk methods for the synthesis of various benzazole derivatives with diverse functional groups.[11–14] Studies show that many of the previously reported methods have some disadvantages, including difficult and dangerous procedures, poor efficiency, and the use of expensive catalysts and raw materials. Given the extensive and interesting chemistry of benzazoles and their diverse applications in the pharmaceutical manufacturing industry, efforts to economically prepare these compounds are important and efficient.[15–17]

Imidates are important organic intermediates used in several synthetic transformations for N-heterocycles, natural products, and metal complexes with a potential catalytic effect.[18–20] The chemistry of imido esters, or imidates, has attracted the attention of scientists for more than a century because of their great utility as tools in the synthesis of heterocyclic compounds.[21–23] Imidates show interesting reactivity with a variety of compounds due to the imide nitrogen atom being a nucleophilic center and the corresponding carbon atom being an electrophilic center. They can form a variety of

[a]Department of Chemistry Education, Farhangian University, P.O. Box 14665-889, Tehran, Iran. E-mail: Y.ahmadi@cfu.ac.ir; Yavahmadi@gmail.com
[b]Department of Physics Education, Farhangian University, P.O. Box 14665-889, Tehran, Iran

complexes with various transition metals, making them valuable pharmaceutically relevant synthons. They have also shown particular importance as intermediates for the synthesis of diverse N-heterocyclic compounds.[24–26] Due to the extensive chemistry of imidates and their numerous applications in the synthesis of natural products and nitrogen-containing heterocyclic compounds, as well as in drug development, there is currently a lack of green and efficient synthetic methods for imidate compounds. Nowadays, it is very necessary to try to synthesize various imidates using cost-effective and simple synthetic methods.

Copper-catalyzed, C–H bond activation reactions are important tools for the construction of carbon-heteroatom bonds.[27–29] Currently, C–H activation is promising to reduce the number of reaction steps and achieve complex chemical products.[30–32] However, the selective cleavage of unactivated C–H bonds is still a difficult research process. Studies have shown that the use of expensive and rare metal catalysts, various additives as oxidants and valuable ligands, and toxic reagents, long reaction times, high-temperature and -pressure conditions, and manipulation of the directing groups are often necessary to carry out the reaction.[33–35] The use of transition metal catalysts for the direct functionalization of inactive C–H bonds is one of the most attractive research topics in organic synthesis. Moreover, the heterofunctionalization of C–H bonds based on atom-economic and economic principles is a step towards the construction of new heterocycle architectures and intermediate compounds. Accordingly, in recent years, a variety of important and complex compounds with diverse functional groups have been synthesized using this new strategy.[36–38]

In previous works, we have attempted to synthesize new heterocyclic compounds using intramolecular C–H activation reactions catalyzed by copper iodide.[39–43] Some of these reactions are demonstrated in Scheme 1, including the synthesis of new heterocyclic compounds from the quinazoline and (trichloromethyl)quinazoline-4(1*H*)-one family.[44,45]

In this work, we studied the synthesis of new benzazoles with imidate skeleton derivatives. The one-pot, Cu-catalyzed, C–H activation reactions of various isocyanides, benzo(thiazole-oxazole-imidazole), and various alcohols under ultrasound conditions at room temperature without the addition of ligands and oxidizing agents are described.[46] The advantages of this method include easy procedures, high availability and low cost of the required materials and catalysts, the achievement of appropriate efficiency (73–91%), performing the reaction under ultrasonic conditions to increase the speed and efficiency of the reaction, and avoidance of the use of ligands, making this approach attractive and outstanding for the synthesis of products.

Initially, we attempted to test the synthesis of phenyl *N*-phenylbenzo[*d*]oxazole-2-carbimidate (**4a**) under different conditions to achieve the optimal conditions for the designed reaction. Through systematic variation of catalysts (CuCl, Cu_2O, CuBr, and CuI), solvents (MeCN, DMF, THF, and acetone), and

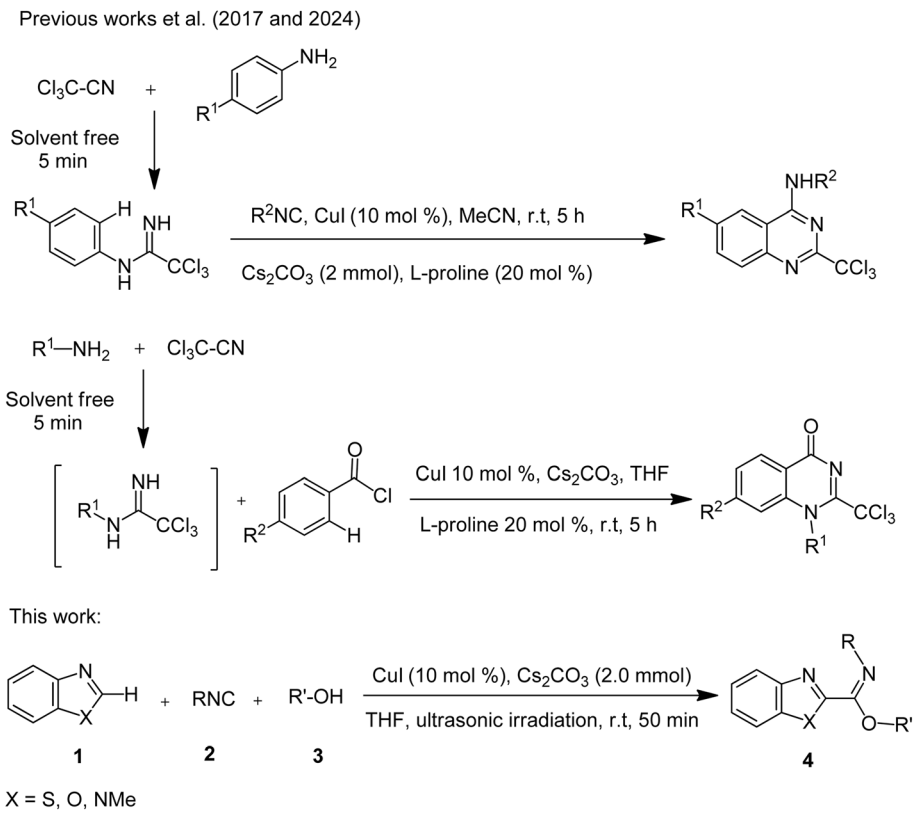

Scheme 1 Comparison of this work (synthesis of various benzazoles with an imidate skeleton by Cu-catalyzed C–H activation reactions) and previous works.

Table 1 Optimization of the reaction conditions for the formation of product **4a** from 1.5 mmol of isocyanides, 1.0 mmol of benzothiazole, 1.0 mmol of phenol, 10 mol% of copper salt as the catalyst, and 2.0 mmol of different bases, under ultrasonic conditions

Entry	Catalyst	Base	Solvent	Yield[a] (%)
1[b]	**CuI**	**Cs_2CO_3**	**THF**	**87**
2	CuI	Cs_2CO_3	MeCN	75
3	CuI	K_2CO_3	DMF	66
4	CuI	KOH	Acetone	50
5	CuBr	Cs_2CO_3	THF	80
6	CuBr	Cs_2CO_3	MeCN	65
7	CuBr	K_2CO_3	DMF	45
8	CuBr	KOH	Acetone	42
9	CuCl	Cs_2CO_3	THF	75
10	CuCl	Cs_2CO_3	MeCN	58
11	CuCl	K_2CO_3	DMF	41
12	CuCl	KOH	Acetone	34
13	Cu_2O	Cs_2CO_3	THF	69
14	Cu_2O	Cs_2CO_3	MeCN	38
15	Cu_2O	K_2CO_3	DMF	30
16	Cu_2O	KOH	Acetone	26
17	Cu	Cs_2CO_3	THF	—
18	Cu	K_2CO_3	MeCN	—
19	—	Cs_2CO_3	MeCN	—
20	—	K_2CO_3	THF	—

[a] Reaction time of 50 min. [b] 5 mol% catalyst, reaction time was 2 h.

bases (K_2CO_3, KOH, and Cs_2CO_3), the optimal conditions were determined as follows: THF solvent, CuI catalyst, and Cs_2CO_3 base. Control experiments (no catalyst and with copper metal) demonstrated the necessity of a copper salt catalyst for the reaction to proceed (see Table 1, entry 17–20). Reducing the CuI catalyst loading from 10 mol% to 5 mol% increased the reaction time from 50 min to 2 hours, highlighting the importance of sufficient catalysts. The optimized conditions (THF, 10 mol% CuI, and 2.0 mmol Cs_2CO_3) achieved a high yield of the desired product within a 50 minute reaction time under ultrasonic conditions. By using these optimized conditions in combination, we were able to further accelerate the reaction and improve the overall yield of the desired product. Therefore, the reaction was tested in THF using 10 mol% of CuI as the catalyst, 2.0 mmol of Cs_2CO_3 as the base, 1.0 mmol of various alcohols, 1.5 mmol of isocyanides, and 1.0 mmol of benzo(thiazole-oxazole-imidazole) (see Table 1).

Considering the results of our previous work on the effectiveness of ultrasonic radiation and the effect of different radiation powers in improving the speed and efficiency of reactions using ultrasound technique, in this study we used ultrasound technique to achieve the optimal conditions for efficiency and reaction time. The results provided in Table 2 confirm that ultrasound plays an important role in improving the efficiency and speed of the reaction.

Applying these optimized conditions to a range of substrates with varied substituents on the aromatic rings demonstrated the broad scope and flexibility of the Cu-catalyzed C–H activation reaction for synthesizing various benzazoles with an imidate functional group from CuI as the catalyst, Cs_2CO_3 as the base, benzo(thiazole-oxazole-imidazole), various alcohols and

Table 2 Effectiveness and importance of ultrasound in product synthesis **4a**

Entry	Isolated yield (%)	Power (W)	Time (min)
1	52	30	80
2	64	40	75
3	76	50	60
4	**87**	**60**	**50**
5	87	70	50
6[a]	74	—	240

[a] Performing the reaction under reflux conditions.

isocyanides with various electron-withdrawing or electron-donating substituents on the aromatic rings (see Table 3).

We used ^{1}H and ^{13}C-NMR, IR, and mass spectral data to characterize the structures of compounds **4a–l**. Spectral studies confirm the successful synthesis of benzazoles with an imidate skeleton. For example, the ^{1}H-NMR spectra of compound **4a**, as well as multiple signals for the phenyl protons, confirm the proposed structure. The ^{13}C NMR spectrum of **4a** exhibited 16 signals in agreement with the proposed structure. The molecular ion peak at $m/z = 314$ in the mass spectrum indicates the molecular mass of the compound.

The proposed reaction pathway is shown step by step in Scheme 2. It seems that the reaction of CuI with benzothiazole **1** in the presence of Cs_2CO_3 as a base under an oxidative addition reaction gives complex **5**. The carbon atom of the isocyanide may be coordinated with copper. Then, by removing the catalyst under a reductive elimination reaction, compound **6** was formed. Finally, the attack of oxygen from phenol as a nucleophile on compound **6** formed the final product **4**.

As a result, a simple, novel, one-pot method for the synthesis of diverse benzazoles with an imidate skeleton *via* a catalyst-

Table 3 Synthesis of various benzazoles with an imidate functional group

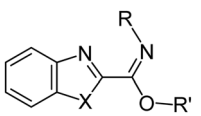

4

Compound	X	R	R′	Yield of 4 (%)
4a	O	Ph	Ph	87
4b	S	Ph	Bn	84
4c	NMe	Ph	Et	82
4d	O	2-Cl-C_6H_4	4-Br-C_6H_4	78
4e	S	2-Cl-C_6H_4	Me	73
4f	NMe	4-Br-C_6H_4	4-Me-C_6H_4	79
4g	O	4-Br-C_6H_4	Bn	80
4h	S	4-Me-C_6H_4	Bn	91
4i	NMe	4-Me-C_6H_4	*t*-Bu	89
4j	O	4-OMe-C_6H_4	*t*-Bu	88
4k	S	Cyclohexyl	Ph	84
4l	NMe	Isopropyl	Me	82

assisted, C–H activation reaction with successful efficiency is reported. The reaction involves three components, namely, isocyanides, benzo(thiazole-oxazole-imidazole), and various alcohols catalyzed by copper(I) iodide for 50 min in THF, resulting in the formation of the desired products with good yields under ultrasound irradiation conditions. In this design, we were able to synthesize and identify a series of different benzazoles with an imidate skeleton using a copper iodide catalyst. The availability of starting materials, simple purification conditions without column chromatography, good efficiency (73–91%), and the avoidance of ligands make this approach attractive for the synthesis of these compounds.

Computational methods

To gain deeper insights into the thermodynamic stability and electronic properties of the synthesized benzazole-based imidate derivatives, density functional theory (DFT) calculations were performed. The primary objective of this computational study was to comparatively evaluate the effect of heteroatom substitutions (X = O, S, N–H, and N–CH_3) on the thermodynamic and electronic properties of the final products. Accordingly, the calculations were carried out exclusively on the optimized structures of the isolated products, and included the evaluation of Gibbs free energies, frontier molecular orbitals, Mulliken charge distributions, molecular electrostatic potentials (MEPs), chemical potentials, and electrophilicity indices. It should be noted that this study was not intended to elucidate the catalytic reaction mechanism; therefore, transition-state searches and activation free-energy calculations for the elementary reaction steps were not performed. Since the experimental reactions were conducted in tetrahydrofuran (THF), solvent effects were explicitly considered using the SMD solvation model to provide a realistic description of the solution-phase environment.

All calculations were performed using the Gaussian software package. Geometry optimizations were conducted at the B3LYP/LANL2DZ level of theory without applying symmetry restrictions in order to allow the complete relaxation of the molecular structures on the potential energy surface. Harmonic vibrational frequency calculations were subsequently carried out at the same level of theory to verify the nature of the optimized structures.[47–51] The absence of imaginary frequencies confirmed that all stationary points correspond to true local minima. Frequency calculations were additionally employed to obtain thermal corrections and thermodynamic parameters under standard conditions (298.15 K and 1 atm).

The solvent environment was modeled using the SMD continuum solvation approach within the self-consistent reaction field (SCRF) formalism, with THF selected as the solvent in accordance with the experimental conditions. This model accounts for both electrostatic and nonelectrostatic solute–solvent interactions, enabling reliable estimation of solution-phase thermodynamic properties.

The calculated thermodynamic parameters, including Gibbs free energy (ΔG), enthalpy (ΔH), and entropy (ΔS), were used to evaluate the relative stability of the investigated benzazole derivatives and to examine the effect of heteroatom substitution on their energetic behavior in solution.[52,55] In addition, frontier molecular orbital analysis was performed through the evaluation of HOMO and LUMO energies, energy gaps, chemical potentials, and electrophilicity indices in order to investigate the influence of heteroatom variation on the electronic structure and global reactivity of the studied systems. The combined thermodynamic and electronic analyses provide a comparative understanding of the stability and reactivity trends observed among the benzoxazole, benzothiazole, benzimidazole, and *N*-methylbenzimidazole derivatives.[53,54]

Computational results

To investigate the influence of heteroatom substitution on the thermodynamic behavior of amidine-functionalized benzazole systems, density functional theory (DFT) calculations were carried out for a series of benzazole derivatives containing different heteroatoms within the heterocyclic framework (X = O, S, N–H, and *N*-methyl). Since the experimental reactions were performed in tetrahydrofuran, solvent effects were incorporated using the SMD solvation model in order to provide a more realistic description of the reaction environment and the relative stabilization of the investigated species in solution.

The Mulliken charge distribution analysis revealed that the highest electron density is predominantly localized on the methyl carbon atom, reflecting its relatively electron-rich nature within the studied systems.[56,57] In contrast, the lowest electron density was observed for the carbon atoms directly bonded to

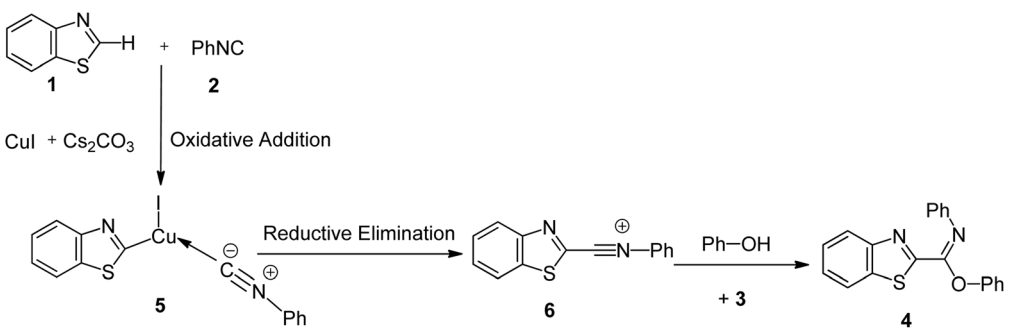

Scheme 2 Possible formation mechanism of compounds **4**.

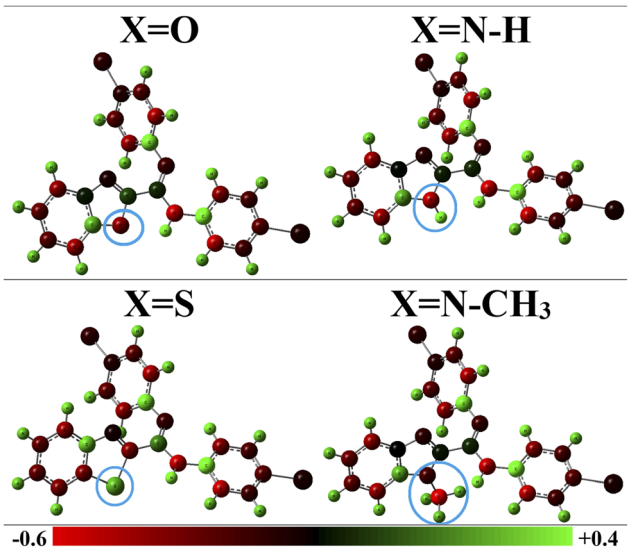

Fig. 1 Optimized geometries of the investigated benzazole-based systems obtained at the B3LYP/LANL2DZ level of theory in THF using the SMD solvation model. The blue circles indicate the corresponding heteroatom/substituent within the benzazole framework (X = O, S, N–H, and N–CH_3). Mulliken charge distributions are displayed on the optimized structures to illustrate the heteroatom-dependent electronic distribution and its influence on the relative thermodynamic stability of the studied systems.

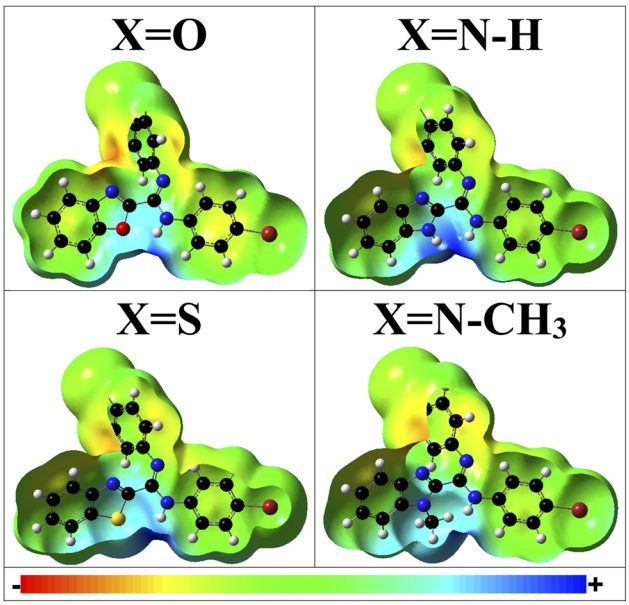

Fig. 2 Molecular electrostatic potential (MEP) maps of the investigated benzazole derivatives (X = O, S, N–H, and N–CH_3) in THF. The color scale represents the potential range from the most negative (red) to most positive (blue) regions, highlighting the influence of heteroatom variation on the surface electronic properties and molecular reactivity.

electronegative heteroatoms, particularly nitrogen atoms, due to their strong electron-withdrawing nature and high electronegativity. This effect is especially pronounced in the benzimidazole-based derivatives, where the presence of nitrogen significantly influences the overall electronic distribution and stabilization of the molecular framework. These variations demonstrate the important role of heteroatom substitution in modulating the electronic properties of the benzazole systems. The optimized structures along with the corresponding Mulliken charge distributions are shown in Fig. 1.

To further visualize the electrophilic and nucleophilic regions and evaluate the impact of heteroatom substitution on the surface reactivity, molecular electrostatic potential (MEP) mapping was performed for the four investigated derivatives. The MEP surfaces provide a clear visual representation of the electronic environment, where the color grading from red (electron-rich) to blue (electron-deficient) illustrates the relative distribution of charge density across the benzazole-imidate framework. This analysis allows for a more comprehensive understanding of how the nature of the heteroatom (X = O, S, N–H, and N–CH_3) modulates the molecular polarity and potential interaction sites within the solvent environment. The resulting MEP maps, calculated at the B3LYP/LANL2DZ level of theory, are presented in Fig. 2.

The synergistic analysis of Mulliken charge distributions (Fig. 1) and MEP maps (Fig. 2) confirms that heteroatom substitution is the primary factor governing the electronic landscape of these benzazole systems. While Fig. 1 highlights the localized atomic-scale electronic shifts—particularly the high electron density on nitrogen-bonded carbons—the MEP surfaces in Fig. 2 demonstrate how these internal shifts translate into global molecular reactivity. Specifically, the oxygen-containing derivative (X = O) exhibits more pronounced polarization than the nitrogen and sulfur analogs, which correlates with its lower HOMO–LUMO gap and higher electrophilicity. The transition from *N*-methyl to oxygen substitution results in a visible expansion of the electron-deficient regions (blue areas), reinforcing the thermodynamic findings that more electronegative heteroatoms enhance the electron-accepting capability of the scaffold. Overall, these computational results provide a robust electronic basis for the observed stability trends and reactivity patterns of the synthesized imidate derivatives.

The optimized structures exhibited clear heteroatom-dependent differences in geometry, electronic distribution, and molecular organization, demonstrating that substitution within the benzazole framework strongly influences the thermodynamic behavior of the investigated systems. Comparative analysis of the calculated thermodynamic parameters revealed that both enthalpic stabilization and entropic effects contribute significantly to the relative stability of the derivatives. In addition, the calculated equilibrium temperatures (T_{eq}), corresponding to the condition $\Delta G = 0$, provided further insights into the balance between enthalpy and entropy for each system. These thermodynamic variations may influence the energetic favorability of amidine formation and help explain the experimentally observed reactivity differences among the studied benzazole substrates. The calculated values of ΔG, ΔH, ΔS, and T_{eq} are summarized in Table 4.

The calculated thermodynamic parameters for the investigated benzazole derivatives are summarized in Table 1. To

Table 4 Calculated thermodynamic parameters for benzazole derivatives containing different heteroatoms/substituents (X), including Gibbs free energy (ΔG), enthalpy (ΔH), entropy (ΔS), and equilibrium temperature (T_{eq}, where $\Delta G = 0$). All values were obtained from DFT calculations in THF using the SMD solvation model

Representative ring	Substituent (X)	ΔG	ΔH	ΔS	T_{eq} (K)
Benzoxazole	O	+1.86	−16.52	−61.62	268.0
Benzimidazole	N–H	+0.38	−16.18	−55.54	291.3
Benzothiazole	S	+0.56	−15.95	−55.36	288.1
N-Methylbenzimidazole	*N*-Methyl	+0.81	−15.91	−56.08	283.7

evaluate the influence of heteroatom substitution on the stability of these systems, density functional theory (DFT) calculations were performed in tetrahydrofuran (THF) using the SMD solvation model. The obtained Gibbs free energy (ΔG), enthalpy (ΔH), and entropy (ΔS) values provide a quantitative basis for comparing the thermodynamic behavior of the different benzazole frameworks. Analysis of these parameters allows a systematic assessment of how variations in the heteroatom (X = O, S, N–H, and N–CH_3) affect the energetic profile and relative stability of the studied structures in solution.

Interpretation of equilibrium temperatures

The calculated equilibrium temperatures correspond to the conditions at which the Gibbs free energy change becomes zero ($\Delta G = 0$), indicating a thermodynamic balance between enthalpic stabilization and entropic destabilization. Below these temperatures, the negative enthalpy contribution dominates and the processes are thermodynamically favorable ($\Delta G < 0$). Above these temperatures, the unfavorable entropy term becomes increasingly significant, leading to positive Gibbs free energy values.

Among the investigated systems, the oxygen-containing derivative exhibits the lowest equilibrium temperature (268 K), reflecting its larger entropy penalty despite favorable enthalpic stabilization. In contrast, the N–H derivative shows the highest equilibrium temperature (291 K), indicating a more balanced enthalpy–entropy relationship. The sulfur and *N*-methyl systems display intermediate behavior. These results further confirm that heteroatom substitution significantly affects the thermodynamic balance and stability of benzazole derivatives in solution.

Thermodynamic analysis of benzazole derivatives

To evaluate the influence of heteroatom substitution on the stability of benzazole frameworks, density functional theory (DFT) calculations were performed for a series of derivatives containing different heteroatoms (X = O, S, N–H, and N–CH_3) in the heterocyclic core. All thermodynamic parameters were calculated in tetrahydrofuran (THF) using the SMD solvation model, and the resulting values of Gibbs free energy (ΔG), enthalpy (ΔH), and entropy (ΔS) are summarized in Table 4.

The comparison of the calculated Gibbs free energies reveals a clear trend in the relative thermodynamic stability of the investigated systems. Among the studied derivatives, the benzimidazole system (X = N–H) exhibits the lowest ΔG value (+0.38 kcal mol^{-1}), indicating the most favorable thermodynamic profile under the modeled conditions. Benzothiazole (X = S) shows a slightly higher value (+0.56 kcal mol^{-1}), suggesting comparable but somewhat reduced stability. The *N*-methylbenzimidazole derivative (X = N–CH_3) displays a moderately higher free energy (+0.81 kcal mol^{-1}), which can be attributed to structural and steric effects introduced by methyl substitution on the nitrogen atom. In contrast, benzoxazole (X = O) exhibits the highest Gibbs free energy (+1.86 kcal mol^{-1}), indicating lower thermodynamic stability among the investigated derivatives.

These results demonstrate that the identity of the heteroatom within the benzazole framework plays an important role in modulating the thermodynamic properties of the system. Subtle differences in electronegativity, electronic distribution, and bonding characteristics influence the relative stability of the heterocycles and contribute to the observed energetic ordering.

Although the N–H-containing derivative exhibits the lowest calculated Gibbs free energy, its experimental yield is comparable to those of the oxygen- and sulfur-containing analogues. This apparent discrepancy arises because the calculated ΔG values describe the relative thermodynamic stability of the isolated products rather than the kinetics of their formation. The reaction yield is primarily determined by the activation barriers of the elementary steps, catalyst performance, possible competing side reactions, and the efficiency of product isolation and purification. Therefore, no direct correlation between the thermodynamic stability of the final products and the experimental yields is necessarily expected. In particular, possible coordination of the N–H functionality to the copper catalyst may influence the catalytic cycle and contribute to the observed experimental behavior.

Enthalpic, entropic, and structural effects

Further insights into the origin of the observed stability trend can be obtained by examining the individual enthalpic and entropic contributions to the Gibbs free energy. The calculated enthalpy values (ΔH) for all investigated systems are negative, ranging from −15.91 to −16.52 kcal mol^{-1}, indicating that the formation of the studied structures is thermodynamically

favorable from an enthalpic standpoint. Among them, benzoxazole exhibits the most negative enthalpy (-16.52 kcal mol^{-1}), suggesting relatively strong intrinsic stabilization at the electronic level.

However, the final Gibbs free energy values are strongly influenced by entropy. The entropy changes (ΔS) are negative for all systems, indicating a decrease in disorder associated with the structural organization in the optimized states. Notably, benzoxazole displays the most negative entropy value (-61.62 cal mol^{-1} K^{-1}), reflecting a larger entropic penalty that offsets its favorable enthalpic contribution and ultimately results in a higher ΔG value. In contrast, benzimidazole and benzothiazole show less negative entropy values (-55.54 and -55.36 cal mol^{-1} K^{-1}, respectively), which contributes to their lower Gibbs free energies.

Structural factors also play a role in this behavior. Variations in heteroatom size, electronegativity, and electronic participation influence both the rigidity of the heterocyclic framework and its interaction with the surrounding solvent environment. The balance between enthalpic stabilization and entropic cost ultimately determines the relative thermodynamic stability of the benzazole derivatives in the THF solution. Together, these results highlight how subtle electronic and structural differences within the benzazole scaffold can significantly influence the overall thermodynamic profile of the system.

Integrated electronic and thermodynamic discussion

To gain deeper insights into the thermodynamic behavior of the investigated benzazole derivatives, global electronic reactivity descriptors were analyzed using frontier molecular orbital theory. The calculated HOMO and LUMO energies, HOMO–LUMO energy gaps, chemical potentials, and electrophilicity indices demonstrate that heteroatom substitution strongly influences the electronic structure and energetic stability of the benzazole framework.

The HOMO–LUMO energy gap (H–L$_{Gap}$), chemical potential (μ), and electrophilicity index (ω) were calculated using the following relationships:[58–60]

$$\text{H–L}_{Gap} = E_{LUMO} - E_{HOMO}. \quad (1)$$

$$\mu = \frac{E_{HOMO} + E_{LUMO}}{2} \quad (2)$$

$$\omega = \frac{\mu^2}{\text{H} - \text{L}_{Gap}} \quad (3)$$

The calculated electronic descriptors for all investigated systems are summarized in Table 5.

The oxygen-containing derivative exhibits the smallest HOMO–LUMO gap (3.58 eV), indicating higher electronic reactivity and lower kinetic stability among the investigated systems. This behavior is accompanied by the lowest LUMO energy and the highest electrophilicity index ($\omega = 4.67$), reflecting a stronger electron-accepting capability arising from the high electronegativity of oxygen. The sulfur derivative displays similar but slightly weaker behavior, with an intermediate HOMO–LUMO gap (3.69 eV) and electrophilicity value ($\omega = 4.39$). In contrast, the nitrogen-containing systems, particularly the *N*-methyl derivative, possess larger HOMO–LUMO gaps, suggesting greater electronic stabilization and lower electrophilicity.

Table 5 Calculated electronic properties of the investigated benzazole derivatives, including frontier molecular orbital energies (E_{HOMO} and E_{LUMO}), HOMO–LUMO gaps, chemical potentials (μ), and electrophilicity indices (ω), obtained at the B3LYP/LANL2DZ level in THF using the SMD solvation model. The energies of E_{HOMO}, E_{LUMO}, the HOMO–LUMO gap, and the chemical potential are reported in electron volts (eV)

Substituent (X)	HOMO	LUMO	H–L$_{Gap}$	μ	ω
O	−5.88	−2.30	3.58	−4.09	4.67
N–H	−5.83	−1.74	4.09	−3.79	3.51
S	−5.87	−2.18	3.69	−4.03	4.39
N-Methyl	−5.84	−1.57	4.27	−3.70	3.21

These electronic trends correlate well with the calculated thermodynamic parameters. Although the oxygen derivative exhibits the most favorable enthalpy value, it also experiences the largest entropic penalty, leading to a comparatively less favorable Gibbs free energy. The enhanced polarity and stronger electronic localization associated with the oxygen atom may contribute to increased solvation effects and reduced configurational freedom in solution, thereby producing a larger entropy loss. Conversely, the *N*-methyl and sulfur derivatives exhibit smaller entropy penalties, resulting in more favorable overall free energies despite slightly less favorable enthalpic stabilization.

The gradual decrease in the HOMO–LUMO gap from *N*-methyl to oxygen substitution is also consistent with the observed increase in electrophilicity and the increasingly negative chemical potential values. These results indicate that the incorporation of more electronegative heteroatoms enhances the electron-accepting ability while modifying the balance between enthalpic stabilization and entropic destabilization in solution. Overall, the combined thermodynamic and electronic analyses demonstrate that heteroatom substitution plays a decisive role in controlling the stability, reactivity, and energetic behavior of benzazole derivatives in THF.

General procedure for the preparation of compounds 4a

A mixture of benzothiazole **1a** (1.0 mmol) and isocyanide **2a** (1.5 mmol), CuI (0.10 mmol), Cs_2CO_3 (2.0 mmol), and phenol **3a** (1.0 mmol) in THF (2 mL) was stirred at r.t. The mixture was sonicated in an ultrasonic apparatus with 60 watts of power for 50 min. The progress of the reaction was monitored by TLC in a *n*-hexane–ethyl acetate (1 : 3) solvent. After the reaction was completed, to remove the copper iodide catalyst from the reaction medium, CH_2Cl_2 (2 mL) and aqueous NH_4Cl solution (3 mL) were added to the reaction mixture and stirred for 10 min. Then the layers were separated. The aqueous layer was extracted with CH_2Cl_2 and the combined organic fractions (Na_2SO_4) were dried

and concentrated under reduced pressure. The resulting solid was isolated by filtration and washed with diethyl ether.

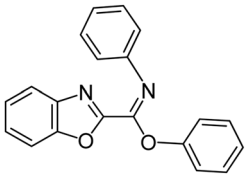

Phenyl *N*-phenylbenzo[*d*]oxazole-2-carbimidate (4a). White powder; yield: 0.27 g (87%); mp: 200–202 °C. IR (KBr) (ν_{max}, cm^{-1}): 1677, 1567, 1466, 1243, 1149. ^{1}H-NMR (500 MHz, $CDCl_3$): $\delta_H = 6.98$ (t, $^3J = 7.8$, 1H, Ar), 7.16 (d, $^3J = 7.5$, 2H, Ar), 7.25 (d, $^3J = 7.6$, 2H, Ar), 7.32 (t, $^3J = 7.6$, 2H, Ar), 7.39 (t, $^3J = 7.5$, 2H, Ar), 7.44–7.48 (m, 3H, Ph), 7.81 (d, $^3J = 7.9$, 1H, Ar), 7.93 (d, $^3J = 7.9$, 1H, Ar). ^{13}C-NMR (125.7 MHz, $CDCl_3$): δ_C = 123.1 (CH), 124.6 (CH), 126.0 (CH), 126.7 (CH), 128.6 (2 CH), 128.7 (CH), 128.8 (2 CH), 130.0 (2 CH), 130.4 (2 CH), 131.0 (CH), 133.8 (C), 134.5 (C), 143.3 (C), 148.5 (C), 152.4 (C), 156.3 (C). MS: *m*/*z* (%) = 314 (M^+, 2), 237 (32), 221 (30), 196 (100), 118 (31), 93 (68), 77 (82). Anal. Calc. for $C_{20}H_{14}N_2O_2$ (314.34): C, 76.42%; H, 4.49%; N, 8.91%. Found: C, 76.44%; H, 4.43%; N, 8.96%.

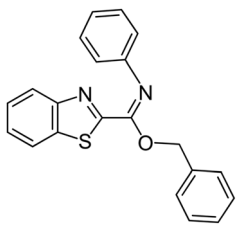

Benzyl *N*-phenylbenzo[*d*]thiazole-2-carbimidate (4b). White powder; yield: 0.22 g (84%); mp: 188–190 °C. IR (KBr) (ν_{max}, cm^{-1}): 1678, 1546, 1469, 1223, 1143. ^{1}H-NMR (500 MHz, $CDCl_3$): $\delta_H = 4.30$ (s, 2H, CH_2), 6.96 (t, $^3J = 7.9$, 1H, Ar), 7.05 (d, $^3J = 7.5$, 2H, Ar), 7.26 (t, $^3J = 7.5$, 2H, Ar), 7.35 (t, $^3J = 7.5$, 2H, Ar), 7.46–7.49 (m, 4H, Ph), 7.67 (t, $^3J = 7.9$, 1H, Ar), 7.82 (d, $^3J = 7.9$, 1H, Ar), 7.93 (d, $^3J = 7.9$, 1H, Ar). ^{13}C-NMR (125.7 MHz, $CDCl_3$): δ_C = 63.7 (CH_2), 125.3 (CH), 125.6 (CH), 125.8 (CH), 125.9 (CH), 128.4 (2 CH), 128.5 (2 CH), 128.6 (2 CH), 129.2 (2 CH), 129.3 (CH), 131.9 (CH), 132.2 (C), 138.1 (C), 143.8 (C), 148.9 (C), 153.9 (C), 158.8 (C). MS: *m*/*z* (%) = 344 (M^+, 10), 267 (39), 253 (61), 134 (100), 91 (34), 77 (98). Anal. Calc. for $C_{21}H_{16}N_2OS$ (344.43): C, 73.23%; H, 4.68%; N, 8.13%. Found: C, 73.25%; H, 4.62%; N, 8.16%.

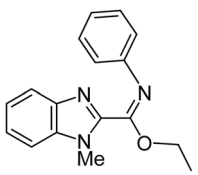

Ethyl 1-methyl-*N*-phenyl-1*H*-benzo[*d*]imidazole-2-carbimidate (4c). Cream oil; yield: 0.23 g (82%). IR (KBr) (ν_{max}, cm^{-1}): 1633, 1550, 1465, 1223, 1149. ^{1}H-NMR (500 MHz, $CDCl_3$): $\delta_H = 1.14$ (t, $^3J = 5.9$, 3H, CH_3), 3.65–3.67 (m, 2H, CH_2), 4.04 (s, 3H, NCH_3), 6.93 (t, $^3J = 7.8$, 1H, Ar), 7.20 (d, $^3J = 7.5$, 2H, Ar), 7.24 (t, $^3J = 7.6$, 1H, Ar), 7.34 (t, $^3J = 7.6$, 2H, Ar), 7.69 (t, $^3J = 7.8$, 1H, Ar), 7.78 (d, $^3J = 7.8$, 1H, Ar), 7.82 (d, $^3J = 7.8$, 1H, Ar). ^{13}C-NMR (125.7 MHz, $CDCl_3$): δ_C = 21.7 (Me), 36.7 (NMe), 63.7 (CH_2), 125.3 (CH), 126.6 (CH), 128.4 (CH), 128.6 (2 CH), 128.7 (CH), 129.1 (CH), 131.0 (2 CH), 134.7 (C), 143.6 (C), 148.4 (C), 153.5 (C), 156.7 (C). MS: *m*/*z* (%) = 279 (M^+, 8), 234 (43), 202 (51), 148 (38), 131 (100), 77 (39), 45 (54). Anal. Calc. for $C_{17}H_{17}N_3O$ (279.34): C, 73.10%; H, 6.13%; N, 15.04%. Found: C, 73.13%; H, 6.17%; N, 15.01%.

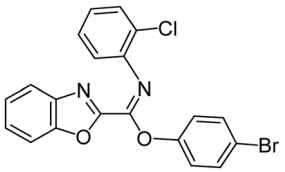

4-Bromophenyl *N*-(2-chlorophenyl) benzo[*d*]oxazole-2-carbimidate (4d). Yellow powder; yield: 0.33 g (78%); mp: 264–266 °C. IR (KBr) (ν_{max}, cm^{-1}): 1678, 1595, 1444, 1233, 1142. ^{1}H-NMR (500 MHz, $CDCl_3$): $\delta_H = 6.97$ (t, $^3J = 7.8$, 1H, Ar), 7.11–7.18 (m, 3H, Ph), 7.25–7.30 (m, 3H, Ph), 7.35 (t, $^3J = 7.8$, 1H, Ar), 7.48 (d, $^3J = 7.8$, 2H, Ar), 7.68 (d, $^3J = 7.9$, 1H, Ar), 7.92 (d, $^3J = 7.9$, 1H, Ar). ^{13}C-NMR (125.7 MHz, $CDCl_3$): δ_C = 120.9 (CH), 121.7 (CH), 125.5 (2 CH), 125.9 (CH), 128.0 (CH), 128.7 (CH), 128.8 (CH), 128.9 (CH), 129.0 (CH), 129.1 (2 CH), 133.2 (C), 138.1 (C), 140.1 (C), 143.8 (C), 148.9 (C), 150.0 (C), 153.3 (C), 158.3 (C). MS: *m*/*z* (%) = 427 (M^+, 1), 314 (41), 270 (89), 154 (100), 118 (43), 111 (86). Anal. Calc. for $C_{20}H_{12}BrClN_2O_2$ (427.68): C, 56.17%; H, 2.83%; N, 6.55%. Found: C, 56.13%; H, 2.87%; N, 6.50%.

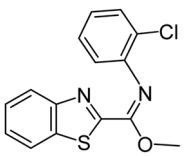

Methyl *N*-(2-chlorophenyl)benzo[*d*]thiazole-2-carbimidate (4e). Cream powder; yield: 0.22 g (73%); mp: 122–124 °C. IR (KBr) (ν_{max}, cm^{-1}): 1683, 1545, 1468, 1251, 1133. ^{1}H-NMR (500 MHz, $CDCl_3$): $\delta_H = 4.24$ (s, 3H, OMe), 6.98 (t, $^3J = 7.9$, 1H, Ar), 7.24–7.29 (m, 3H, Ph), 7.37 (t, $^3J = 7.9$, 1H, Ar), 7.67–7.69 (m, 2H, Ph), 7.94 (d, $^3J = 7.9$, 1H, Ar). ^{13}C-NMR (125.7 MHz, $CDCl_3$): δ_C = 55.7 (OMe), 125.9 (CH), 128.7 (CH), 128.8 (CH), 128.9 (CH), 129.1 (CH), 129.4 (CH), 129.6 (CH), 131.9 (CH), 138.1 (C), 143.8 (C), 148.8 (C), 151.9 (C), 156.0 (C), 158.7 (C). MS: *m*/*z* (%) = 302 (M^+, 2), 271 (72), 191 (66), 168 (32), 134 (45), 111 (100), 31 (43). Anal. Calc. for $C_{15}H_{11}ClN_2OS$ (302.78): C, 59.50%; H, 3.66%; N, 9.25%. Found: C, 59.53%; H, 3.62%; N, 9.28%.

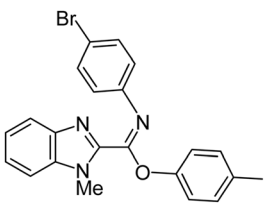

***p*-Tolyl *N*-(4-bromophenyl)-1-methyl-1*H*-benzo[*d*]imidazole-2-carbimidate (4f).** Yellow powder; yield: 0.33 g (79%); mp: 209–211 °C. IR (KBr) (ν_{max}, cm^{-1}): 1667, 1599, 1465, 1243, 1149.

^{1}H-NMR (500 MHz, $CDCl_3$): δ_H = 2.44 (s, 3H, CH_3), 3.55 (s, 3H, NCH_3), 6.98 (t, ^3J = 7.8, 1H, Ar), 7.24–7.29 (m, 4H, Ph), 7.37 (d, ^3J = 7.6, 2H, Ar), 7.48–7.50 (m, 3H, Ph), 7.68 (d, ^3J = 7.8, 1H, Ar), 7.94 (d, ^3J = 7.8, 1H, Ar). ^{13}C-NMR (125.7 MHz, $CDCl_3$): δ_C = 21.3 (Me), 36.6 (NCH_3), 125.5 (CH), 125.9 (C), 128.7 (2 CH), 128.8 (CH), 128.9 (CH), 129.3 (2 CH), 129.4 (2 CH), 129.6 (CH), 131.9 (2 CH), 133.2 (C), 138.1 (C), 143.8 (C), 148.3 (C), 150.1 (C), 154.5 (C), 158.2 (C). MS: *m*/*z* (%) = 420 (M^+, 2), 328 (31), 312 (64), 264 (29), 111 (100), 154 (73), 107 (30), 91 (82). Anal. Calc. for $C_{22}H_{18}BrN_3O$ (420.30): C, 62.87%; H, 4.32%; N, 10.00%. Found: C, 62.83%; H, 4.36%; N, 10.04%.

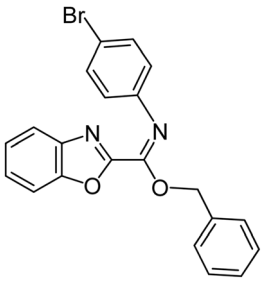

Benzyl *N*-(4-bromophenyl)benzo[*d*]oxazole-2-carbimidate (4g). Cream powder; yield: 0.33 g (80%); mp: 199–201 °C. IR (KBr) (ν_{max}, cm^{-1}): 1687, 1594, 1430, 1263, 1144. ^{1}H-NMR (500 MHz, $CDCl_3$): δ_H = 4.33 (s, 2H, CH_2), 6.99 (t, ^3J = 7.9, 1H, Ar), 7.25 (d, ^3J = 7.8, 2H, Ar), 7.34–7.40 (m, 6H, Ph), 7.48 (d, ^3J = 7.6, 2H, Ar), 7.65 (d, ^3J = 7.9, 1H, Ar), 7.93 (d, ^3J = 7.9, 1H, Ar). ^{13}C-NMR (125.7 MHz, $CDCl_3$): δ_C = 59.5 (OCH_2), 121.3 (CH), 124.5 (CH), 126.7 (C), 127.5 (2 CH), 127.9 (2 CH), 128.5 (2 CH), 128.7 (2 CH), 129.4 (CH), 131.9 (2 CH), 133.8 (C), 134.5 (C), 143.4 (C), 148.7 (C), 152.5 (C), 158.5 (C). MS: *m*/*z* (%) = 407 (M^+, 1), 314 (34), 298 (29), 251 (40), 154 (39), 118 (81), 107 (100), 91 (49). Anal. Calc. for $C_{21}H_{15}BrN_2O_2$ (407.26): C, 61.93%; H, 3.71%; N, 6.88%. Found: C, 61.95%; H, 3.73%; N, 6.84%.

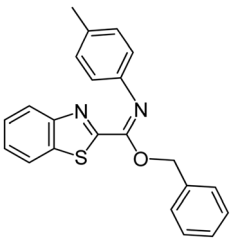

Benzyl *N*-*p*-tolylbenzo[*d*]thiazole-2-carbimidate (4h). Cream powder; yield: 0.32 g (91%); mp: 187–189 °C. IR (KBr) (ν_{max},-cm^{-1}): 1678, 1593, 1468, 1263, 1143. ^{1}H-NMR (500 MHz, $CDCl_3$): δ_H = 2.81 (s, 3H, CH_3), 4.22 (s, 2H, CH_2), 6.99 (t, ^3J = 7.9, 1H, Ar), 7.15–7.20 (m, 3H, Ph), 7.28 (d, ^3J = 7.6, 2H, Ar), 7.31–7.39 (m, 3H, Ph), 7.49 (d, ^3J = 7.6, 2H, Ar), 7.66 (d, ^3J = 7.9, 1H, Ar), 7.92 (d, ^3J = 7.9, 1H, Ar). ^{13}C-NMR (125.7 MHz, $CDCl_3$): δ_C = 31.4 (Me), 60.4 (OCH_2), 121.6 (CH), 124.0 (C), 126.0 (2 CH), 127.5 (2 CH), 127.9 (2 CH), 128.5 (2 CH), 128.7 (2 CH), 129.4 (CH), 131.2 (CH), 132.8 (C), 134.3 (C), 142.4 (C), 148.4 (C), 153.4 (C), 158.2 (C). MS: *m*/*z* (%) = 358 (M^+, 4), 251 (50), 224 (11), 107 (32), 91 (100). Anal. Calc. for $C_{22}H_{18}N_2OS$ (358.46): C, 73.71%; H, 5.06%; N, 7.82%. Found: C, 73.73%; H, 5.02%; N, 7.80%.

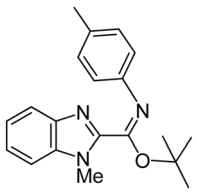

***Tert*-Butyl 1-methyl-*N*-(*p*-tolyl)-1*H*-benzo[*d*]imidazole-2-carbimidate (4i).** Yellow oil; yield: 0.28 g (89%). IR (KBr) (ν_{max}, cm^{-1}): 1667, 1592, 1470, 1204, 1175. ^{1}H-NMR (500 MHz, $CDCl_3$): δ_H = 1.31 (s, 9H, 3 CH_3), 2.43 (s, 3H, CH_3), 3.61 (s, 3H, NCH_3), 6.97 (t, ^3J = 7.8, 1H, Ar), 7.26 (d, ^3J = 7.5, 2H, Ar), 7.36 (t, ^3J = 7.8, 1H, Ar), 7.47 (d, ^3J = 7.5, 2H, Ar), 7.67 (d, ^3J = 7.8, 1H, Ar), 7.91 (d, ^3J = 7.8, 1H, Ar). ^{13}C-NMR (125.7 MHz, $CDCl_3$): δ_C = 22.4 (3 Me), 29.3 (Me), 38.9 (NCH_3), 60.0 (C), 121.7 (CH), 125.5 (CH), 129.0 (CH), 129.1 (2 CH), 129.3 (2 CH), 131.9 (CH), 133.2 (C), 138.1 (C), 143.8 (C), 148.9 (C), 155.6 (C), 158.9 (C). MS: *m*/*z* (%) = 321 (M^+, 8), 287 (39), 190 (62), 131 (73), 91 (100), 73 (78). Anal. Calc. for $C_{20}H_{23}N_3O$ (321.42): C, 74.74%; H, 7.21%; N, 13.07%. Found: C, 74.71%; H, 7.24%; N, 13.03%.

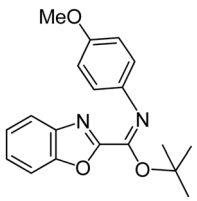

***Tert*-Butyl *N*-(4-methoxyphenyl) benzo[*d*]oxazole-2-carbimidate (4j).** Cream oil; yield: 0.28 g (88%). IR (KBr) (ν_{max}, cm^{-1}): 1677, 1593, 1467, 1205, 1146. ^{1}H-NMR (500 MHz, $CDCl_3$): δ_H = 1.23 (s, 9H, 3 CH_3), 4.08 (s, 3H, OCH_3), 6.96 (t, ^3J = 7.9, 1H, Ar), 7.24 (d, ^3J = 7.4, 2H, Ar), 7.35 (t, ^3J = 7.9, 1H, Ar), 7.46 (d, ^3J = 7.4, 2H, Ar), 7.68 (d, ^3J = 7.9, 1H, Ar), 7.93 (d, ^3J = 7.9, 1H, Ar). ^{13}C-NMR (125.7 MHz, $CDCl_3$): δ_C = 21.9 (3 Me), 55.5 (OMe), 60.6 (C), 125.9 (CH), 128.9 (CH), 129.0 (2 CH), 129.1 (2 CH), 129.2 (CH), 129.3 (CH), 133.2 (C), 138.1 (C), 143.8 (C), 148.9 (C), 152.5 (C), 158.1 (C). MS: *m*/*z* (%) = 324 (M^+, 11), 251 (36), 217 (61), 206 (54), 107 (50), 107 (100), 73 (39). Anal. Calc. for $C_{19}H_{20}N_2O_3$ (324.37): C, 70.35%; H, 6.21%; N, 8.64%. Found: C, 70.32%; H, 6.25%; N, 8.62%.

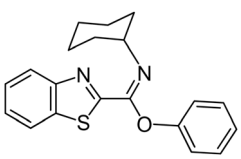

Phenyl *N*-cyclohexylbenzo[*d*]thiazole-2-carbimidate (4k). Cream oil; yield: 0.28 g (84%). IR (KBr) (ν_{max}, cm^{-1}): 1650, 1540, 1466, 1209, 1141. ^{1}H-NMR (500 MHz, $CDCl_3$): δ_H = 1.10–1.17 (m, 2H, CH_2), 1.74–1.78 (m, 4H, CH_2), 1.80–1.82 (m, 4H, CH_2), 2.60–2.65 (m, 1H, CH), 6.97 (t, ^3J = 7.6, 1H, Ar), 7.27 (t, ^3J = 7.6, 2H, Ar), 7.36 (d, ^3J = 7.6, 2H, Ar), 7.46–7.49 (m, 2H, Ph), 7.69 (d, ^3J = 7.8, 1H, Ar), 7.92 (d, ^3J = 7.8, 1H, Ar). ^{13}C-NMR (125.7 MHz, $CDCl_3$): δ_C = 13.5 (CH_2), 21.7 (2 CH_2), 22.1 (2 CH_2), 31.7 (CH), 125.9 (CH), 128.8 (CH), 129.0 (2 CH), 129.1 (2 CH), 129.4 (CH), 131.8 (CH), 133.2 (CH), 138.8 (C), 143.8 (C), 148.9 (C), 151.5 (C),

157.8 (C). MS: m/z (%) = 336 (M^+, 8), 259 (40), 253 (42), 243 (66), 107 (97), 83 (42). Anal. Calc. for $C_{20}H_{20}N_2OS$ (336.45): C, 71.40%; H, 5.99%; N, 8.33%. Found: C, 71.42%; H, 5.94%; N, 8.30%.

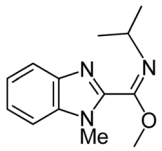

Methyl *N*-isopropyl-1-methyl-1*H*-benzo[*d*]imidazole-2-carbimidate (4l). Yellow oil; yield: 0.19 g (82%). IR (KBr) (ν_{max}, cm^{-1}): 1653, 1590, 1460, 1203, 1145. ^{1}H-NMR (500 MHz, $CDCl_3$): δ_H = 1.80 (d, ^3J = 5.8, 6H, 2 CH_3), 3.22 (s, 3H, NCH_3), 3.50–3.53 (m, 1H, CH), 4.00 (s, 3H, OCH_3), 6.94 (t, ^3J = 7.7, 1H, Ar), 7.23 (t, ^3J = 7.7, 1H, Ar), 7.42 (d, ^3J = 7.7, 1H, Ar), 7.51 (d, ^3J = 7.7, 1H, Ar). ^{13}C-NMR (125.7 MHz, $CDCl_3$): δ_C = 21.8 (2 Me), 37.7 (NMe), 40.4 (CH), 55.7 (OMe), 125.6 (CH), 126.5 (CH), 128.1 (CH), 129.1 (CH), 142.5 (C), 148.5 (C), 152.6 (C), 158.7 (C). MS: m/z (%) = 270 (M^+, 7), 188 (24), 131 (64), 100 (100), 43 (47). Anal. Calc. for $C_{13}H_{17}N_3O$ (231.29): C, 67.51%; H, 7.41%; N, 18.17%. Found: C, 67.55%; H, 7.43%; N, 18.14%.

Conclusion

In summary, an efficient copper-catalyzed one-pot three-component C–H activation protocol under ultrasonic irradiation was developed for the synthesis of benzazole-based imidate derivatives. The reaction proceeds under mild conditions without the need for additional ligands or oxidizing agents and provides the desired products in good to excellent yields. The use of readily available starting materials, short reaction time, and simple purification procedure highlight the practical advantages of this synthetic approach.

Furthermore, density functional theory (DFT) calculations were performed to investigate the thermodynamic stability and electronic properties of the synthesized benzazole-based imidate derivatives containing different heteroatoms (X = O, S, N–H, and N–CH_3). The calculated Gibbs free energies, enthalpies, and entropies revealed that heteroatom substitution significantly influences the relative thermodynamic stability of the investigated products. Among the studied derivatives, the N–H-containing system exhibited the lowest Gibbs free energy, indicating the most favorable thermodynamic stability within the investigated series, whereas the oxygen-containing derivative showed a larger entropy penalty despite its favorable enthalpic contribution.

Frontier molecular orbital analysis, molecular electrostatic potential mapping, and electronic descriptor calculations demonstrated that heteroatom variation also affects the electronic structure and global properties of the benzazole framework. In particular, oxygen substitution resulted in a smaller HOMO–LUMO gap and higher electrophilicity compared with the other investigated systems, indicating enhanced electron-accepting characteristics. Overall, the combined experimental and computational results demonstrate that heteroatom substitution is an important factor in controlling the thermodynamic and electronic properties of benzazole-based imidate derivatives. The present DFT study provides molecular-level insights into the properties of the isolated products and complements the experimental findings without addressing the detailed catalytic reaction mechanism.

Author contributions

Yavar Ahmadi: project administration, writing – original draft, formal analysis, visualization. Manijeh Nematpour: data curation, writing – reviewing and editing, methodology. Mohammad Qasemnazhand: investigation, writing – reviewing and editing, software.

Conflicts of interest

There are no conflicts to declare.

Data availability

The datasets generated and/or analysed during the current study are available in the [supporting documents] repository.

Supplementary information (SI): detailed experimental procedures, characterization data, spectroscopic data, and computational details, including DFT calculation results, for the synthesized compounds. See DOI: https://doi.org/10.1039/d6ra05617b.

Notes and references

1 P. Hu, W. Li, Y. Li, Y. Su, B. Zhang and L. Shen, *Catal. Lett.*, 2024, **154**, 2396.
2 T. Su, S. Xie, B. Li, J. Yian, L. Huang and X. Li, *Synlett*, 2015, **26**, 215–220.
3 X. Gao, J. Liu, X. Zuo, X. Feng and Y. Gao, *Molecules*, 2020, **25**, 1675.
4 S. Fujiwara, Y. Asanuma, T. Shinike and N. Kambe, *J. Org. Chem.*, 2007, **72**, 8087.
5 M. K. Singh, R. Tilak, G. Nath, S. K. Awasthi and A. Agarwal, *Eur. J. Med. Chem.*, 2013, **63**, 635.
6 V. Gandin, P. Khalkar, J. Braude and A. P. Fernandes, *Free Radical Biol. Med.*, 2018, **127**, 80.
7 K. N. Venugopala, M. A. Khedr, M. Pillay, S. K. Nayak, S. Chandrashekharappa, B. E. Aldhubiab, S. Harsha, M. Attimard and B. Odhav, *J. Biomol. Struct. Dyn.*, 2019, **37**, 1830.
8 B. Berk, Y. A. Tahirovic, E. F. Bülbül and S. N. Biltekin, *Acta Pharm. Sci.*, 2017, **55**, 17.
9 P. F. Santos, L. V. Reis, P. Almeida, J. P. Serrano, A. S. Oliveira and L. F. V. Ferreira, *J. Photochem. Photobiol., A*, 2004, **163**, 267.
10 V. N. Telvekar, V. K. Bairwa, K. Satardekar and A. Bellubi, *Bioorg. Med. Chem. Lett.*, 2012, **22**, 649.
11 M. Kaname, M. Minoura and H. Sashida, *Tetrahedron Lett.*, 2011, **52**, 505.
12 S. Redon, Y. Kabri, M. D. Crozet and P. Vanelle, *Tetrahedron Lett.*, 2014, **55**, 5052.

13 N. R. Conley, A. Dragulescu-Andrasi, J. Rao and W. E. Moerner, *Angew. Chem., Int. Ed.*, 2012, **51**, 1.
14 A. L. Braga, F. Vargas, J. A. Sehnem and R. C. Braga, *J. Org. Chem.*, 2005, **70**, 9021.
15 D. M. Freudendahl, S. A. Shahzad and T. Wirth, *Eur. J. Org. Chem.*, 2009, 1649.
16 M. Yadav and V. P. Singh, *J. Org. Chem.*, 2023, **88**, 16934.
17 K. Kobayashi and Y. Yokoi, *Helv. Chim. Acta*, 2012, **95**, 761.
18 R. Thakur, Y. Jaiswal and A. Kumar, *Org. Biomol. Chem.*, 2019, **17**, 9829.
19 G. Borah, B. Dam and B. K. Patel, *ChemistrySelect*, 2022, **7**, e202104583.
20 K. A. Rykaczewski, E. R. Wearing, D. E. Blackmun and C. S. Schindler, *Nat. Synth.*, 2022, **1**, 24–36.
21 A. G. Chaidali and I. N. Lykakis, *Molecules*, 2023, **28**, 3321.
22 K. Watanabe, N. Kogoshi, H. Miki and Y. Torisawa, *Synth. Commun.*, 2009, **39**, 2008.
23 L. Ptiček, L. Hok, P. Grbčić, F. Topić, M. Cetina, K. Rissanen, S. K. Pavelić, R. Vianello and L. Racané, *Org. Biomol. Chem.*, 2021, **19**, 2784.
24 M. K. Arachchi and H. M. Nguyen, *Adv. Synth. Catal.*, 2021, **363**, 4239.
25 F. T. Liu, S. Wang, Y. S. Chen, J. Y. Miao, B. Zhao and Z. M. Lin, *Org. Chem. Front.*, 2025, **12**, 97.
26 C. R. Davis, N. Ichiishi, B. J. Burke and J. S. Tedrow, *J. Org. Chem.*, 2025, **90**, 1905.
27 J. Wencel-Delord, T. Dröge, F. Liu and F. Glorius, *Chem. Soc. Rev.*, 2011, **40**, 4740.
28 J. F. Hartwig and M. A. Larsen, *ACS Cent. Sci.*, 2016, **2**, 281.
29 N. Kuhl, M. N. Hopkinson, J. Wencel-Delord and F. Glorius, *Angew. Chem., Int. Ed.*, 2012, **51**, 10236.
30 L. M. Jin, P. Xu, J. Xie and X. P. Zhang, *J. Am. Chem. Soc.*, 2020, **142**, 20828.
31 U. Dhawa, C. Tian, T. Wdowik, J. C. A. Oliveira, J. Hao and L. Ackermann, *Angew. Chem., Int. Ed.*, 2020, **59**, 13451.
32 A. M. Kazerouni, Q. A. McKoy and S. B. Blakey, *Chem. Commun.*, 2020, **56**, 13287.
33 S. Santoro, F. Ferlin, L. Luciani, L. Ackermann and L. Vaccaro, *Green Chem.*, 2017, **19**, 1601.
34 T. Gensch, M. N. Hopkinson, F. Glorius and J. Wencel-Delord, *Chem. Soc. Rev.*, 2016, **45**, 2900.
35 P. Gandeepan, T. Müller, D. Zell, G. Cera, S. Warratz and L. Ackermann, *Chem. Rev.*, 2019, **119**, 2192.
36 J. Kim, D. Kim and S. Chang, *J. Am. Chem. Soc.*, 2020, **142**, 19052.
37 A. K. Chaturvedi, R. K. Shukla and C. M. R. Volla, *Chem. Sci.*, 2024, **15**, 6544.
38 J. Liao, D. Kong, X. Gao, R. Zhai, X. Chen and S. Wang, *Molecules*, 2024, **29**, 3567.
39 M. Nematpour and Y. Ahmadi, *Synopen*, 2026, **10**(03), 190.
40 A. H. Massoudi, I. Amini, A. Ramazani, F. Zeinali Nasrabadi and Y. Ahmadi, *Bull. Korean Chem. Soc.*, 2012, **33**, 39.
41 M. Nematpour, E. Rezaee, M. Jahani and S. A. Tabatabai, *Ultrason. Sonochem.*, 2019, **50**, 1.
42 Y. Ahmadi, M. Nematpour and H. Ahankar, *Results Chem.*, 2026, **27**, 103452.
43 H. Ahankar, A. Ramazani and Y. Ahmadi, *Phosphorus, Sulfur Silicon Relat. Elem.*, 2014, **189**, 914.
44 M. Nematpour, *J. Heterocycl. Chem.*, 2024, **61**, 1914.
45 M. Nematpour, E. Rezaee, M. Jahani and S. A. Tabatabai, *Synlett*, 2017, **28**, 1441.
46 M. Nematpour and Y. Ahmadi, *Tetrahedron*, 2025, **186**, 134883.
47 M. Qasemnazhand, F. Khoeini, F. Marsusi and A. Ben Ahmed, *Mater. Today Commun.*, 2026, **52**, 114971.
48 M. Qasemnazhand, F. Khoeini, M. A. Bazrafshan and A. I. Ayesh, *J. Phys. Chem. Solids*, 2025, **197**, 112441.
49 K. Naderia, M. Sajjadi, M. Qasemnazhand, A. Ghaemi, M. Nasrollahzadeh and H. Ghafuri, *Chem. Eng. J.*, 2026, **527**, 171605.
50 Y. Ahmadi, H. Teymourinia, S. M. Hosseininezhad and A. Ramazani, *Inorg. Chem. Commun.*, 2024, **162**, 112153.
51 Y. Ahmadi, M. Manafi Moghadam and A. Ramazani, *Chem. Methodol.*, 2025, **9**(8), 702–714.
52 M. Ahmadi, A. Ghaemi and M. Qasemnazhand, *Sci. Rep.*, 2023, **13**(1), 7150.
53 M. Ahmadi, F. Bahmanzadegan, M. Qasemnazhand, A. Ghaemi and H. Ramezanipour Penchah, *Sci. Rep.*, 2024, **14**(1), 13595.
54 A. Zarei, Y. Ahmadi and A. Ramazani, *J. Mol. Struct.*, 2025, **1319**, 139499.
55 M. Sheikhi, Y. Ahmadi, S. Kaviani and S. Shahab, *Struct. Chem.*, 2021, **32**, 1181–1196.
56 M. Qasemnazhand, F. Khoeini and M. Badakhshan, *Mater. Today Chem.*, 2023, **28**, 101383.
57 M. Qasemnazhand, F. Khoeini and F. Marsusi, *Results Phys.*, 2022, **43**, 106066.
58 F. Bahmanzadgan, A. Ghaemi, M. Qasemnazhand and M. Molaee, *Sci. Rep.*, 2025, **15**(1), 15595.
59 M. Qasemnazhand, F. Khoeini and F. Marsusi, *Sci. Rep.*, 2021, **11**(1), 2511.
60 N. Karimi, S. Kamalinahad, M. Qasemnazhand, M. Alizadeh and N. Ajalli, *Int. J. Hydrogen Energy*, 2025, **168**, 151018.